Manuscript Details

Manuscript number	ENGEO_2018_1686
Title	Sphericity measures of sand grains
Article type	Research Paper

Abstract

The sphericity of a grain should measure the similitude of its shape with that of a sphere. Sphericity as shape descriptor is of traditional interest for sedimentology. Now it has gained also interest to facilitate discrete element modelling of granular materials. True sphericity was initially defined by a surface ratio that requires three-dimensional (3D) grain surface measurement. That kind of measurement has been practically impossible until recently and, as a consequence, a number of alternative 3D measures and 2D proxies were proposed. In this work we present results from a study of grain shape based on x-ray tomography of two different sand specimens, containing more than 110.000 particles altogether. Sphericity measures were systematically obtained for all grains. 2D proxy measures were also obtained in samples of oriented and not-oriented grains. It is shown that the 2D proxy best correlated with true sphericity is perimeter sphericity, whereas the traditional Krumbein-Sloss chart proxy is poorly correlated. 2D measures acquired through minor axis projection are more closely related to 3D measures than those acquired using random projections.

Keywords	sand; shape; statistics; microtomography; image analysis.
Taxonomy	Soil Properties, Engineering Geology, Sand, Soil Morphology
Corresponding Author	Riccardo Rorato
Corresponding Author's Institution	Universitat Politecnica de Catalunya (UPC)
Order of Authors	Riccardo Rorato, Marcos Arroyo, Edward Andò, Antonio Gens
Suggested reviewers	Fatin Altuhafi, ignazio cavarretta, Budi Zhao, Stefano Utili

Submission Files Included in this PDF

File Name [File Type]

Highlights.docx [Highlights]

Rorato Arroyo et al. - sphericity measures of sand grains.pdf [Manuscript File]

To view all the submission files, including those not included in the PDF, click on the manuscript title on your EVISE Homepage, then click 'Download zip file'.

Research Data Related to this Submission

There are no linked research data sets for this submission. The following reason is given:
Data will be made available on request

Highlights:

- 3D shape descriptors for 110.000 sand grains are obtained
- True sphericity is independent of particle size
- True sphericity distributions show significant variability and skew
- Maximum projection perimeter sphericity (2D) is a good 2D proxy for true sphericity
- Krumbein-Sloss 2D sphericity is poorly correlated with true sphericity

Sphericity measures of sand grains

Rorato R[1]., Arroyo M[1]., Andò E[2]., Gens A[1].

Riccardo Rorato *(corresponding author)*
riccardo.rorato@upc.edu

Marcos Arroyo Alvarez de Toledo
marcos.arroyo@upc.edu

Edward Carlo Giorgio Andò
edward.ando@3sr-grenoble.fr

Antonio Gens Solé
antonio.gens@upc.edu

[1] Universitat Politécnica de Catalunya (UPC), Barcelona (Spain) - Department of Civil and Environmental Engineering
[2] Université Grenoble Alpes, CNRS, Grenoble INP, Laboratoire 3SR, Grenoble (France)

Declaration of interest: None

Abstract

The sphericity of a grain should measure the similitude of its shape with that of a sphere. Sphericity as shape descriptor is of traditional interest for sedimentology. Now it has gained also interest to facilitate discrete element modelling of granular materials. True sphericity was initially defined by a surface ratio that requires three-dimensional (3D) grain surface measurement. That kind of measurement has been practically impossible until recently and, as a consequence, a number of alternative 3D measures and 2D proxies were proposed. In this work we present results from a study of grain shape based on x-ray tomography of two different sand specimens, containing more than 110.000 particles altogether. Sphericity measures were systematically obtained for all grains. 2D proxy measures were also obtained in samples of oriented and not-oriented grains. It is shown that the 2D proxy best correlated with true sphericity is perimeter sphericity, whereas

the traditional Krumbein-Sloss chart proxy is poorly correlated. 2D measures acquired through minor axis projection are more closely related to 3D measures than those acquired using random projections.

Keywords: sand; shape; statistics; microtomography; image analysis.

1 Introduction

Numerous studies show that particle shape has a significant influence on properties of engineering interest for granular soils (Chang et al., 2018; Cho et al., 2006a; Holubec and D'Appolonia, 1973; Liu and Lehane, 2013; Santamarina and Cho, 2004; Vaid et al., 1985; Yang and Luo, 2015). To incorporate this knowledge into geotechnical practice it is necessary to measure shape. Although particle shape is not simple to define, an operational definition taken from a more general context (Iyer et al., 2005) is useful here: shape is the geometrical information of an object left once location, size and orientation are given. Unfortunately, there is no general agreement on how best to quantify and convey that geometrical information i.e. which technique (Uday et al., 2013) or shape descriptors to use. A large number of proposals are available and, as noted before (Bowman et al., 2001; Cavarretta, 2009; Rodriguez, 2012), this creates terminological confusion as well as some conceptual difficulties.

The definition above suggests that shape descriptors should be size-independent. Beyond that, the selection of shape descriptors may be best guided by the application i.e. by considering the purpose for which shape information is being gathered. Shape descriptors have been traditionally used to classify particles, for instance as a preliminary step in the design of experimental studies, but also for material control purposes (aggregates, ballast), or as a key to infer past sedimentary

processes. Within this context, the trend has been towards separate descriptors based on measurement scale considerations. Thus Barret (Barret, 1980) defined shape as the combination of three aspects: *form*, measured at particle scale, *roundness*, measured at an intermediate scale, and *surface texture*, measured at small scale. These are meant to be independent properties, hence suitable descriptors for these three aspects should not be strongly correlated.

Independent descriptors can also be obtained by using appropriate functional basis to represent a generic surface as the sum of a series. The series coefficients are independent from one another and unambiguously defined. For granular soils spherical harmonics have been used (Mollon and Zhao, 2013; Ouhbi et al., 2016; Zhou et al., 2015). This approach may be well adapted for automated reconstruction of particle shape, which is of interest in some discrete computational approaches. On the other hand, particles series coefficients are relatively abstract descriptors, difficult to interpret and relate to more traditional descriptors. This is inconvenient, as traditional descriptors are easily measured and well ingrained in practice.

Scale separation is not the only possible criterion to select a suitable shape descriptor. Wadell (Wadell, 1932) argued that similitude to a sphere or *sphericity* was a more appropriate criterion. The reason was that spheres were limiting cases for several physical mechanism of general interest, such as sedimentation through a fluid or rolling motion. To this we can add a new reason: spheres are of much interest for discrete element method (DEM) computations, because they are the most economical shape to use. Sphericity may be then used as input to simplify calibration of DEM models (Rorato et al., 2018).

The sphericity measure originally proposed by Wadell (1932) required measurement of particle surface area. For individual particles, this kind of measurement has not been feasible until very recently. Before that, sphericity could only be evaluated by proxy, using simpler measures, sometimes based on two-dimensional projections of the particle outline. Again, lack of consensus has resulted in a large variety of proxy measures.

Sphericity proxy measures are still in use and are likely to remain so, because they are more economical to acquire than direct measurements. It is therefore of interest to examine which of these proxies (if any) is best correlated with the harder to obtain 3D value. This is one objective of this work, for which we exploit a large database of sand grain 3D images, acquired through micro-computed tomography (µCT). The size of the database examined also allows to obtain statistically significant sphericity distributions. In what follows we first describe the different measures of sphericity that have been proposed. Afterwards we describe the measurement methodology before presenting and discussing the results obtained.

2 Background

2.1 True sphericity and its proxies

The surface ratio proposed by Wadell (Wadell, 1932) was called *true sphericity* and denoted by Ψ. It was defined as the surface ratio of a sphere having the same volume as the particle to the surface of the particle itself (see Table 1 and 2).

Name	Symbol	Definition	Reference
True Sphericity	Ψ	$\frac{s_n}{S}$	(Wadell, 1932)
Flatness index	FI	c/b	(Zingg, 1935)
Elongation index	EI	b/a	(Zingg, 1935)
Intercept sphericity	Ψ_{int}	$\sqrt[3]{\frac{bc}{a^2}} = \sqrt[3]{FI\left(EI\right)^2}$	(Krumbein, 1941)
Operational Sphericity	Ψ_{op}	$\sqrt[3]{\frac{V}{V_{cm}}} = \frac{D_n}{D_{cm}} \approx \frac{D_n}{a}$	(Krumbein, 1941)
Convexity	Co	V/V_{CH}	(Fonseca et al. 2012)
Alshibli Sphericity	Ψ_{al}	V/V_{iM}	(Alshibli et al., 2015)

Table 1: Three dimensional shape descriptors (see Table 2 for symbol definitions)

Shape property	Symbol	Equivalent diameter
Volume	V	D_n
Surface area	S	
Surface area of the equivalent sphere (same volume)	s_n	
Maximum, intermediate, minimum lengths	a, b, c	
Convex hull volume	V_{CH}	D_{CH}
Volume of the maximum inscribed sphere	V_{iM}	D_{iM}
Volume of the minimum circum-scribed sphere	V_{cm}	D_{cm}

Table 2: Fundamental measures from which 3D shape descriptors are derived

Because of the isoperimetric inequality, Ψ is strictly bounded by 1. True sphericity was deemed (Wadell, 1933) more comprehensive than form measures based on a few "representative" diameters. In fact, true sphericity is affected by shape features at all scales, (Barret, 1980; Zhao and Wang, 2016) certainly by form and roundness, but also, if measurement resolution allows for it, by surface texture.

Wadell true sphericity had a serious drawback: it required the surface area of irregular grains, measurement of which is very challenging. Since only average measurements using surface absorption techniques were possible at the time, Wadell himself proposed (Wadell, 1935) a practical alternative: obtain first a plane projection of the particle, then compute the ratio of a diameter of the circle which area equal to the projection to that of its maximum circumscribing circle. This (see Table 3) is what was later called *diameter sphericity*, and as it is measured in 2D, it cannot be more than an approximation.

Name	Symbol	Formula
Area sphericity	s_A	$s_A = \frac{d_n^2}{d_{cm}^2}$

Name	Symbol	Formula
Diameter sphericity	s_D	$s_D = \frac{d_n}{d_{cm}} = \sqrt{s_A}$
Circle ratio sphericity	s_C	$s_D = \frac{d_{iM}}{d_{cm}}$
Perimeter sphericity	s_P	$s_P = \frac{p_n}{p}$
KS sphericity	s_{KS}	$s_{KS} = \frac{d_2}{d_1}$

112 *Table 3: 2D sphericity proxies, terminology following Zheng & Hryciw (2015)*

Shape property	Symbol	Equivalent diameter	Equivalent perimeter
Projected area	a_n	d_n	p_n
maximum & minimum dimensions of projected area	d_1, d_2		
Diameter of minimum circumscribing circle	d_{cm}		
Diameter of maximum inscribed circle	d_{iM}		
Projected perimeter	p		

113 *Table 4: Fundamental measures from which 2D sphericity proxies are derived*

114 The projection plane was specified as that containing the longest and intermediate perpendicular
115 bounding dimensions of the particle (here denoted *a, b*). The direction of projection was perpen-
116 dicular, i.e. parallel to the smallest characteristic dimension, *c*. These linear dimensions charac-
117 terize length, width and breadth. Their ratios (elongation ratio *EI* and flatness, *FI*, see Table 1) or
118 combinations thereof are generally used to describe *form* (Blott and Pye, 2008).

119

120 Measures along three perpendicular axes cannot uniquely identify spheres, as they are only sen-
121 sitive to a lesser degree of symmetry (orthotropy) than that present in a sphere. On the other hand,
122 length, width and breadth are relatively easy to measure in particles above gravel size. Krumbein
123 (Krumbein, 1941) proposed *intercept sphericity*, Ψ_{int} as a proxy for sphericity based on form ratios

(see Table 1). He showed that, when averaging many measurements, it was equal to an *operational sphericity*, (Ψ_{op}, Table 1), a measure he also proposed, defining it as ratio of particle volume to volume of the circumscribing sphere.

Krumbein (1941) also included a method to assess roundness, by comparison with photographs of reference grains. That idea was later extended by Krumbein and Sloss (Krumbein and Sloss, 1963) to a double entry graphic reference chart, which could be used to assign both roundness and sphericity, by visual comparison. The graphic chart method is somewhat slow and imprecise, but pragmatic and simple. It gained much success and is still frequently in use (e.g. Santamarina and Cho 2004, Cho et al. 2006).

It was not fully clear which 2D proxy measure had been used to assign values to the examples in the Krumbein (Krumbein and Sloss, 1963) chart. Alternative 2D proxies, different from diameter sphericity, had been proposed by that time (Table 3 and Table 4). Somewhat surprisingly, recent work by Zheng & Hryciw (Zheng and Hryciw, 2015) demonstrated that the "sphericity" numbers in the charts (S_{KS} in Table 3) corresponded closely with the width to length ratio, which, if maximum size projection was used to obtain the 2D image, is simply the elongation index.

Indeed, when considering 2D proxy measures one important question is which projection direction is employed. Traditional specifications (Krumbein, 1941; Wadell, 1933) required projection area maximization and, therefore, some control on particle alignment. However, this is not possible in some automated systems, which operate on a dynamic setting, by imaging flowing particles (Altuhafi et al., 2012; Lin et al., 2017). These systems are fast and very efficient but result in randomly-oriented projections.

2.2 Measuring true sphericity

Individual particle measurements of volume and surface area are now possible. Hayakawa (Hayakawa and Oguchi, 2005) applied laser scanning to gravel particles and obtained 50 values of several 3D shape descriptors, including Ψ, Ψ_{int} and Ψ_{op}. They noted poor correlation between these three indexes. Komba (Komba et al., 2013) used the same technique on six different gravel-sized aggregates, acquiring data on 150 particles of each. They obtained material-dependent correlations between Ψ and a sum of low-order spherical harmonic coefficients. Sun (Sun et al., 2014) laser-scanned 180 ballast particles of sizes 15-50 mm to explore the relation between several shape descriptors and size. Their results show how EI, FI and Ψ_{op} increase with particle size; on the other hand, Ψ was relatively independent of size.

For sand-sized particles laser scanning appears unpractical. Although other techniques are possible (e.g. stereophotogrammetry; Nadimi and Fonseca 2017) most work has been based on tomography. Some studies have been of a demonstrative nature, using very few grains. Thus Lin and Miller (2005) obtained Ψ values from 20 grain samples of several granular materials. Zhao and Wang (2016) measured Ψ and extended the technique to map local curvatures on 30 grains of sand.

More numerous data were presented by Fonseca (Fonseca et al., 2012), which analysed several specimens containing about 3000 grains each. They measured Ψ but the algorithm employed was somewhat imprecise resulting in many values above 1. They also noted poor correlation of Ψ with both flatness and elongation indices obtained from dynamic (hence randomly-oriented) measurements. They also used a different 3D descriptor, *convexity* (Co, Table 1) that appeared simpler to measure.

Alshibli (Alshibli et al., 2015) introduced new definitions of 3D sphericity (Ψ_{al} , Table 1) and roundness as well as new proxies for them in 2D projection. Histograms were presented, but the number of grains examined was not mentioned. No significant correlation was found between the

175 newly introduced 3D indexes and their 2D proxies. On the other hand, Suh (Suh et al., 2017) did
176 note a good correlation (on average) between a 3D measure (operational sphericity, Ψ_{op}) and its
177 2D equivalent (diameter sphericity, Ψ_{S_D}), while analysing 7 sands at 350 grains each.

178 3 Methodology

179 3.1 Data acquisition

180 The starting point for this study are two sand specimens, approximately 10mm diameter and
181 20mm height, presented in (Andò, 2013) at Laboratoire 3SR (Grenoble, France). Both specimens
182 were prepared by dry pluviation and then subject to triaxial compression under 100kPa of confin-
183 ing pressure. The triaxial tests were performed *in-situ* within the x-ray scanner at Laboratoire
184 3SR.
185 The first specimen (HNEA01) is comprised with Hostun HN31 sand. Hostun is a quartz sand used
186 in many previous laboratory studies (Calvetti et al., 2004; Desrues et al., 1996; Schanz and
187 Vermeer, 1996). Its grains appear very irregular, see Figure 1a. The grain size distribution of the
188 material tested here, shown in Figure 1b, is very narrow ($C_U = 1.41$), with a D_{50} equal to 338 μm,
189 as given by the supplier (Sibelco).

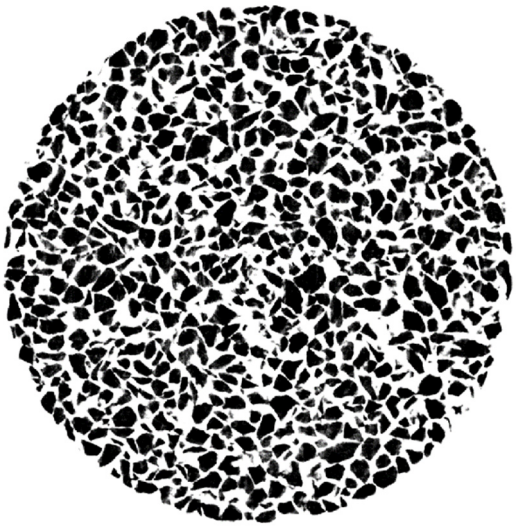

(a)

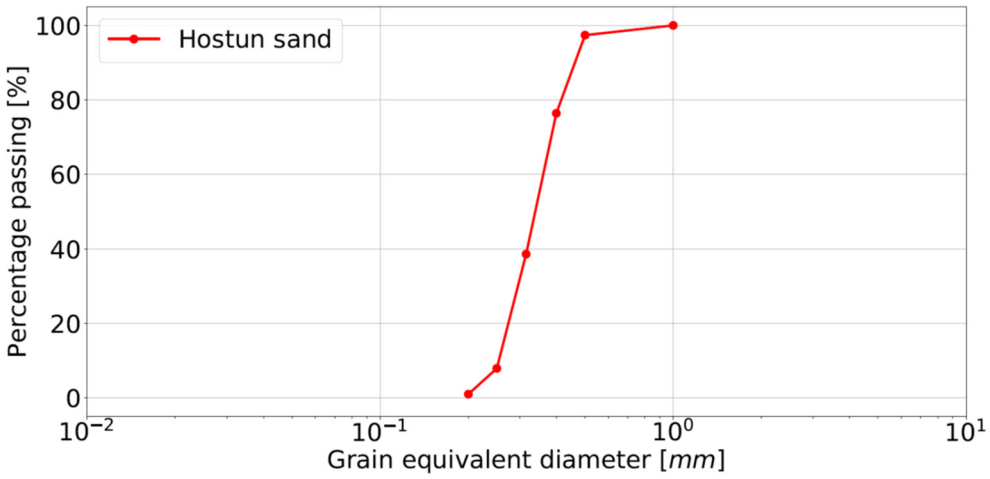

(b)

Figure 1: Horizontal section of the scanned Hostun sand specimen (a). Grain Size Distribution of Hostun sand from sieving by the manufacturer Sibleco (Andò, 2013) *(b)*

The second specimen (COEA04) is comprised with Caicos ooids. This sand comes from the Caicos Islands, in the British West Indies. Ooids grow in marine environment from small seeds like shell fragments or calcite grains that subsequently become larger because some material gets attached to the grain while rolling or by precipitation over the surface. This mechanism generates round-looking particles (Figure 2a). Caicos ooids is a rare material for which little data is available beyond that reported by Andò (Andò 2013). Caicos ooids are made of calcium carbonate (CaCO3) minerals: the 96% is aragonite and the rest is calcite. The specimen grain size distribution (Figure 2b) is close to that of HNEA01, being also poorly graded ($C_U = 1.39$) with a D_{50} of 420 μm.

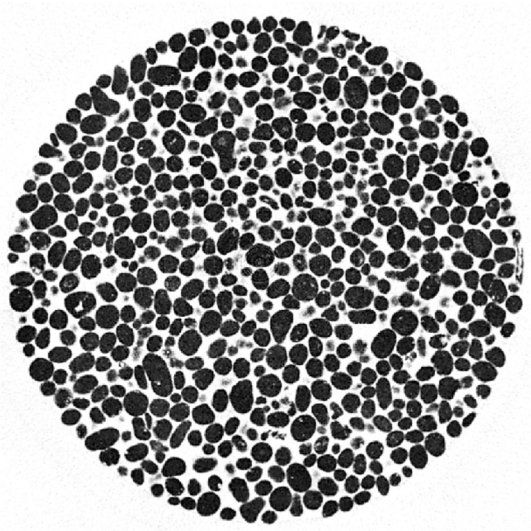

(a)

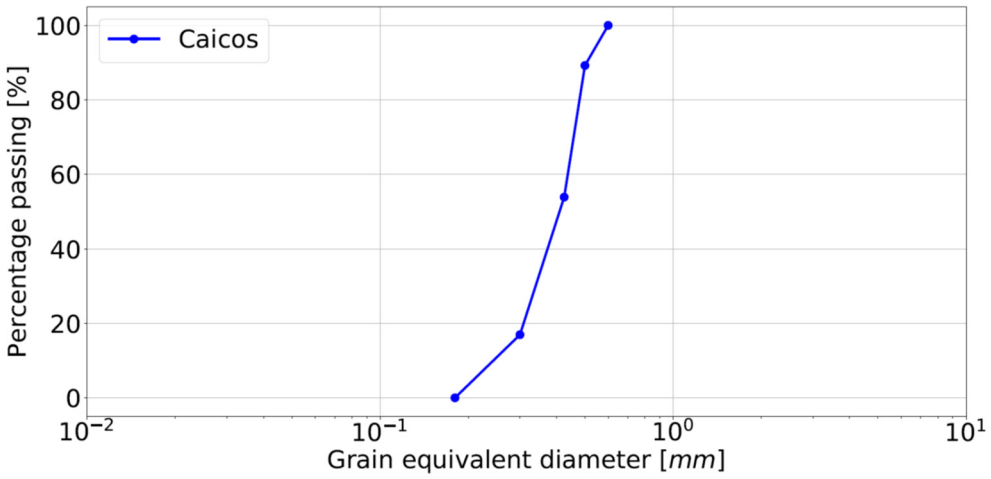

(b)

Figure 2: Horizontal section of the scanned Caicos sand specimen (a). Grain Size Distribution of Caicos sand from sieving by Exxon (Andò, 2013) *(b)*

The specimens described were scanned several times during the triaxial test. Unless otherwise noted all the results presented below refer to the first scan of the specimens, done after cell confinement was applied but before starting triaxial compression.

The pixel size selected to image the studied sands is 15.56 μm/px, to maintain a field of view of approximately 30.5 mm × 23.0 mm. For the specimens analysed this results in about 30 pixels across a grain. Further details of the scanning equipment and tomographic image acquisition procedures have been presented in (Andò, 2013).

3.2 Spatial (3D) measures of shape

The 3D tomographic images are simply grey-scale images, in which the greyscale of each voxel (i.e. three-dimensional pixel) represents the x-rays attenuation coefficient. To individuate grains it is necessary to binarise, separate and label each voxel of the tomographic images (Andò et al., 2012). 3D labelled voxel subsets representing a grain can be subsequently extracted and analysed to obtain some geometrical properties (e.g. volume, surface area, inertia tensor). These operations require numerical image analysis.

The numerical image analysis in this work was based on "ad hoc" python scripts, making use of its scientific libraries *Numpy* (Oliphant, 2006) and *Scipy* (Jones et al., 2001). The general flow diagram of the operations is presented in Figure 3. The algorithms followed for binarisation, separation and labelling have been described elsewhere (Andò, 2013; Andò et al., 2012). Curiously, the most computationally expensive operation by far (around 80% of the total calculation time) was also the simplest: extraction of a labelled voxel subset corresponding to a grain. The reason is that it required a loop through the whole specimen billion-sized voxel collection.

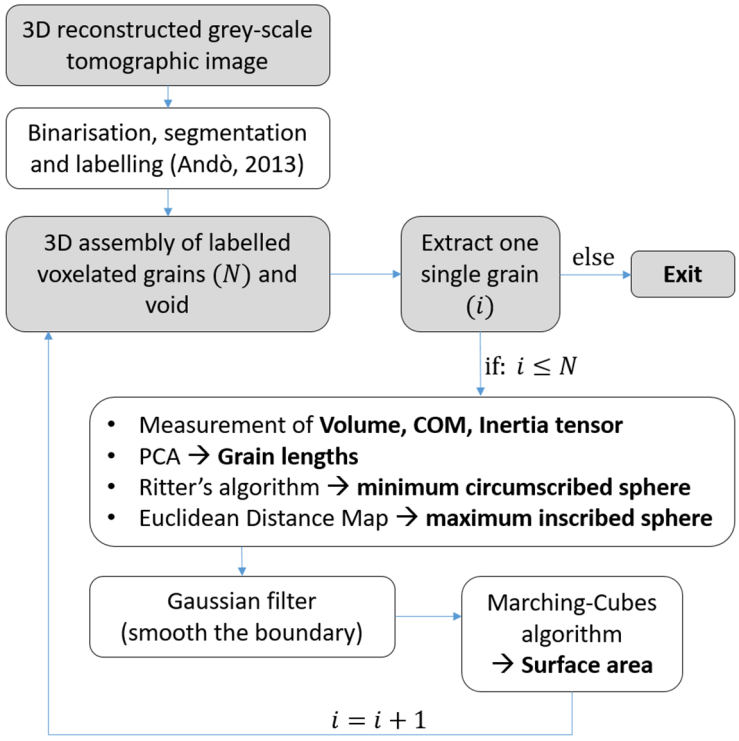

Figure 3: Flow diagram of image treatment operations

Grain volume is obtained adding up labelled voxels. It was assumed that material density is uniform to compute the centre of mass (COM) and inertia tensor of each grain. Grain projections on the principal axis of the inertia tensor were used to define maximum, intermediate and minimum grain lengths. This procedure was also employed by Lin (Lin and Miller, 2005) and, using statistical terminology, it is sometimes described (Alshibli et al., 2015; Fonseca et al., 2012) as Principal Component Analysis (PCA).

The minimum circumscribed sphere and the maximum inscribed sphere are calculated making use of Ritter's algorithm and the Euclidean distance transform, respectively. In this algorithm (Ritter, 1990) an Euclidean distance transform is applied to binarised images, labelling each voxel of the image with its distance to the nearest boundary, thus implicitly defining the centre and radius of the maximum inscribed sphere.

Following Lin & Miller (2005) particle surface area was quantified using the Marching Cubes (MC) algorithm (Lorensen and Cline, 1987) on the labelled grain. MC operated on a grain voxel collection whose surface had been previously smoothed using a Gaussian filter. The filter defines continuous iso-surfaces that can be given as input to the MC algorithm. The MC output is a mesh of triangular elements, whose areas are added up to compute grain surface. The computational time requested by these operations is only 2% of the total calculation time, which makes the MC algorithm very efficient. The convex hull is evaluated directly through a predefined Scipy function (based on the *Qhull* library, Barber and Dobkin 1996). Table 2 lists the shape properties numerically evaluated for each grain.

3.3 Projected (2D) measures of shape

2D measures of shape were acquired on all particles using as projection direction that of the minor principal axis (i.e. projecting the particle outline on the plane containing the larger and intermediate axes, also called the "*plane of greatest stability*"). Suh (Suh et al., 2017) demonstrated that this kind of projection results in 2D shape measures within 5% of the values obtained when particles are displayed on a flat surface (i.e. when they are under equilibrium under self-weight).

For comparison purposes, randomly oriented particle projections were also obtained for a subset of particles of each sand. To do so, all the particles have been projected on a fixed vertical plane, but maintaining the particle in-specimen orientation. The specimens were built using a dry pluviation procedure (Andò, 2013) and it is assumed that this resulted in random particle orientations.

Once the projected outline of the particle was obtained, similar (simplified) algorithms employed for the three-dimensional case (Chapter 3.2) were used to measure bi-dimensional geometrical quantities (Table 4) that, when combined, result in the 2D sphericity descriptors listed in Table 3.

In both cases (*randomly* and *not-randomly* oriented grain projections), the grain label is preserved from the three-dimensional sample, therefore 2D and 3D shape parameters can be directly compared and statistically studied in order to explore potential correlates between them (Section 4.4).

3.4 Validation

The previous procedures were validated in two different ways. The first one was by comparing some results with those obtained using the commercial software Visilog (Bernard et al., 2011). Visilog uses a different algorithm for the surface area calculation. It applies a reduction coefficient to the sum of the boundary voxel faces areas. The average difference for the surface area calculation for the grains in the Hostun specimen was 2.6%. However, the MC algorithm proved more robust, achieving computation for many thousands of particles where Visilog failed. The particle characteristic lengths are obtained by Visilog searching the maximum/minimum Feret diameters over a range of random orientations. The Feret diameters are conceptually different form the lengths established through inertial analysis; however, the values obtained were typically close, never differing more than 6%.

A second validation was performed by checking the difference between the numerical results and the analytical solutions of some artificial shapes. Binarised spheres and prolate/oblate spheroids were built with similar resolution to that of the sand particle images analysed in this study. Results obtained from application of the numerical procedures were compared with the analytical solutions for volume, surface area, moment of inertia, principal directions of inertia, particle lengths, maximum inscribed sphere and minimum circumscribed. All comparisons were favourable with

differences never exceeding 5% (highest deviation given by the Ritter's algorithm for the minimum circumscribed sphere calculation). The error was insensitive to the initial orientation of the artificial shapes, confirming the reliability of the algorithms used.

4 Results

4.1 Size distributions

After labelling was completed, a total of 48.612 and 65.056 particles were identified in the 3D tomographic images of the Hostun (specimen HNEA01) and of the Caicos (specimen COEA04), respectively. Figure 4 shows the histograms of the particle volume for both the specimens HNEA01 and COEA04. The histogram of grain volumes measured by Andò (2013) on a different Caicos specimen (COEA01) is also shown in Figure 4b for comparison.

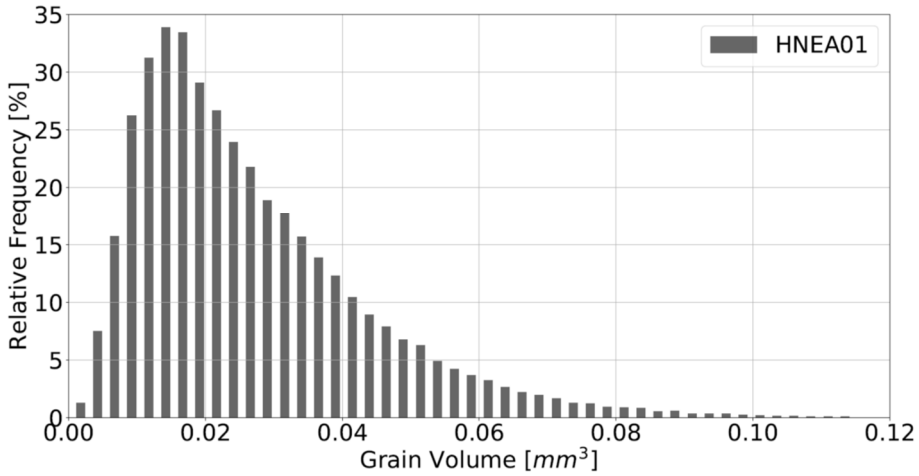

(a)

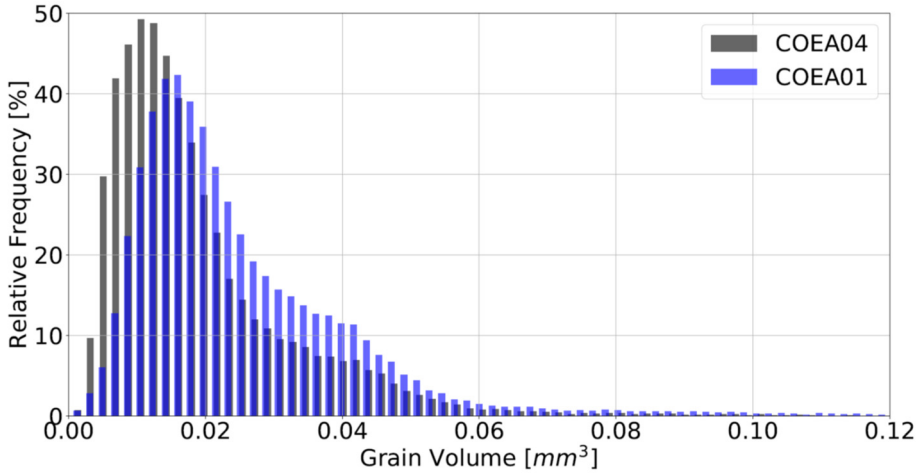

(b)

Figure 4: Histogram of the particles volumes in specimens HNEA01 (a) and COEA04 versus COEA01 (from Andò, 2013) (b)

To compare with sieve-based measures of PSD, volumes are substituted by the *equivalent grain diameter* (the diameter of the sphere having the same volume as the grain). For Hostun sand (Figure 5a) the image-based GSD is very similar to the sieving one as measured by the manufacturer "Sibelco France". Regarding Caicos ooids (Figure 5b), the image-based GSD of COEA04 locates between the sieving curves obtained by Exxon and Laboratoire 3SR. The distributions are similar, although the image-based procedure results in a much smoother curve than what results from a sieve analysis in which only a few discrete sieves were employed.

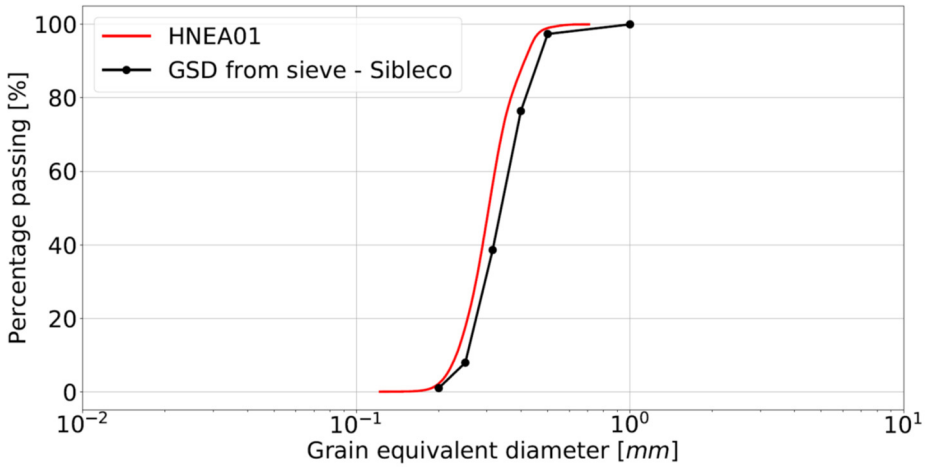

(a)

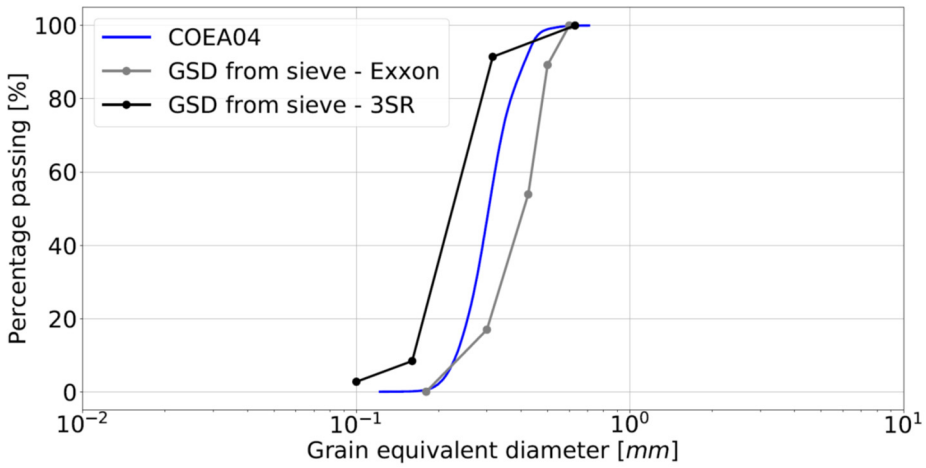

(b)

Figure 5: GSD of HNEA01 (numerical) compared to the one of the manufacturer (a). GSD of COEA04 (numerical) compared to the GSDs measured by Exxon and Laboratoire 3SR (b)

4.2 Shape descriptors: distributions

Shape descriptors were calculated for all the grains contained within both the specimens of Caicos and Hostun sands. Therefore, it is possible to plot histograms of the two sands on the same graph and calculate some statistics.

Table 5, Table 6 and Table 7 list some statistics (i.e. mean, standard deviation, skew and coefficient of variation) of the 3D (Table 5) and 2D (Table 6-7) shape descriptors for both Hostun and Caicos sands. For the 2D case, results are separately presented for the randomly oriented projection (Table 6) and for the oriented projection onto the planes of greatest stability (Table 7).

Name	**Mean** *Hostun* *Caicos*	**St. Dev.** *Hostun* *Caicos*	**Skew** *Hostun* *Caicos*	**CV** *Hostun* *Caicos*
Volume (mm^3)	0.027 0.025	0.017 0.017	1.534 2.31	0.63 0.68
True Sphericity	0.82 0.94	0.06 0.04	-0.75 -1.89	0.07 0.04
Flatness index	0.73 0.85	0.14 0.09	-0.22 -0.65	0.19 0.11

Elongation index	0.76	0.12	-0.24	0.16
	0.80	0.11	-0.65	0.14
Intercept sphericity	0.74	0.09	-0.18	0.12
	0.81	0.08	-0.64	0.10
Operational Sphericity	0.58	0.07	-0.09	0.12
	0.71	0.09	-0.45	0.13
Convexity	0.79	0.08	-1.00	0.10
	0.92	0.06	-2.10	0.06
Alshibli Sphericity	2.08	1.05	2.34	0.51
	0.75	0.09	-0.18	0.12

Table 5: Statistics of the 3D shape descriptors for the two sands at the initial state

Name	**Mean**	**St. Dev.**	**Skew**	**CV**
	Hostun	*Hostun*	*Hostun*	*Hostun*
	Caicos	*Caicos*	*Caicos*	*Caicos*
Area sphericity	0.60	0.12	-0.36	0.20
	0.75	0.12	-0.68	0.16
Diameter sphericity	0.76	0.08	-0.63	0.11
	0.88	0.07	-0.95	0.08
Circle ratio sphericity	0.59	0.11	-0.43	0.19
	0.72	0.11	-0.75	0.15
Perimeter sphericity	0.84	0.05	-0.64	0.06
	0.92	0.04	-1.22	0.04
KS sphericity	0.65	0.12	-0.22	0.18
	0.70	0.13	-0.70	0.19

Table 6: Statistics of the 2D shape descriptors for the two sands (obtained from randomly oriented projections)

Name	**Mean**	**St. Dev.**	**Skew**	**CV**
	Hostun	*Hostun*	*Hostun*	*Hostun*
	Caicos	*Caicos*	*Caicos*	*Caicos*
Area sphericity	0.66	0.10	-0.39	0.15
	0.77	0.10	-0.82	0.13
Diameter sphericity	0.81	0.07	-0.61	0.09
	0.88	0.06	1.05	0.07
Circle ratio sphericity	0.65	0.09	-0.37	0.14
	0.75	0.11	0.86	0.15

Perimeter sphericity	0.85	0.05	-0.86	0.06
	0.92	0.05	-1.70	0.05
KS sphericity	0.76	0.12	-0.25	0.16
	0.80	0.12	-0.78	0.15

Table 7: Statistics of the 2D shape descriptors for the two sands (obtained from projections oriented along the minor principal axis)

Random orientation introduced a significant bias, decreasing the mean values for all 2D parameters. Random particle orientation also increased the variability of almost all 2D shape measures, except that of perimeter sphericity.

Most 3D sphericity measures show a significant negative skew. As for variability it should be noted that the coefficient of variation is not very well adapted to interval bounded measures that represent some distance, like true sphericity. For a uniform distribution (i.e. completely random) true sphericity distribution in the interval 0-1 the CV will be of only 17%, so that the 7% of Hostun is symptomatic of substantial true sphericity variability. Indeed, in most measures the quarried Hostun sand shows a slightly large variability, whereas Caicos shows a more intense skew.

The sketches of four selected grains characterised by the lowest and highest *degree of true sphericity* (ψ) for both, Caicos ooids and Hostun sand, are plotted in Figure 6. The results appear intuitively satisfactory, in that the lesser ψ values correspond to distinctly unspherical shapes (which may correspond to a single grain or perhaps several that the thresholding algorithm failed to separate). The practical range of ψ is therefore rather narrow, a known limitation of this descriptor (Barret, 1980).

	Minimum ψ	Maximum ψ
Hostun	Grain "38536" : $\psi = 0.5075$ 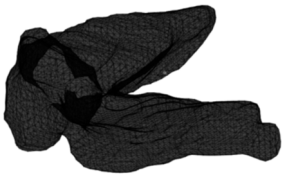	Grain "25161" : $\psi = 0.9753$ 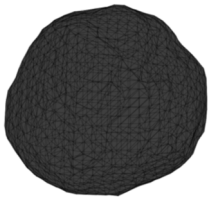
Caicos	Grain "1536" : $\psi = 0.5667$ 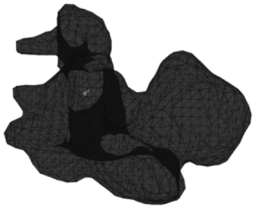	Grain "5866" : $\psi = 0.9998$ 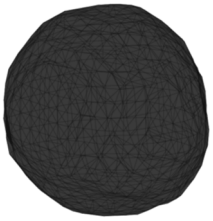

Figure 6: Grains having the extreme values of Degree of True Sphericity

Normalised histograms of *true sphericity* are reported in Figure 7. As expected, values for Caicos sand (mean $\Psi = 0.94$) are substantially higher than those for Hostun sand (mean $\Psi = 0.82$). Moreover, the histogram of Caicos is more narrowly distributed and skewed, as it flattens against the upper limit of 1, whereas the Hostun histogram is more broadly distributed.

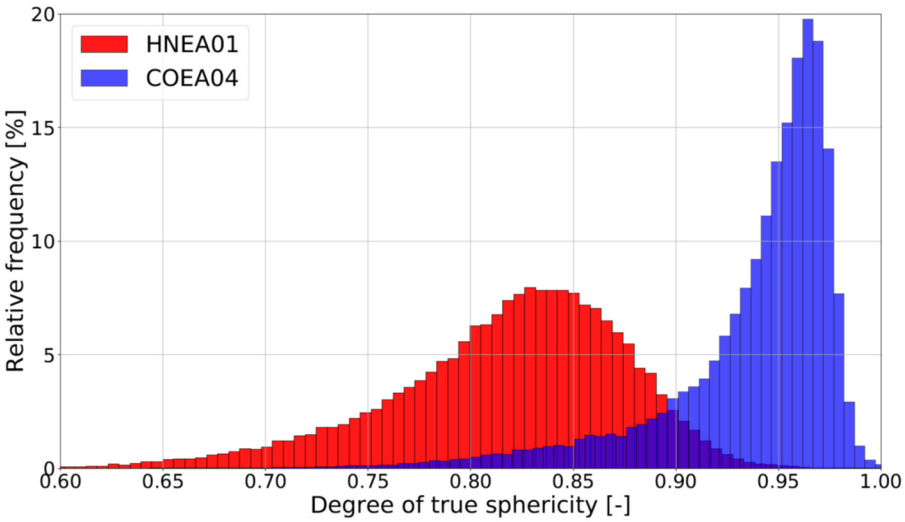

Figure 7: Normalised histograms of true sphericity

Alshibli et al. (2015) presented some shape data for Hostun sand. The mean true sphericity obtained here for Hostun is not far from the 0.77 value they reported. Figure 8 shows a more detailed

comparison, now between the histogram of the Alshibli sphericity index (Ψ_{al}) as reported by Alshibli (2015) and that obtained from this study. Somewhat higher values are obtained here, but taking into account that different sand specimens, image acquisition systems and data treatment algorithms are employed, the agreement between the two distributions is satisfactory.

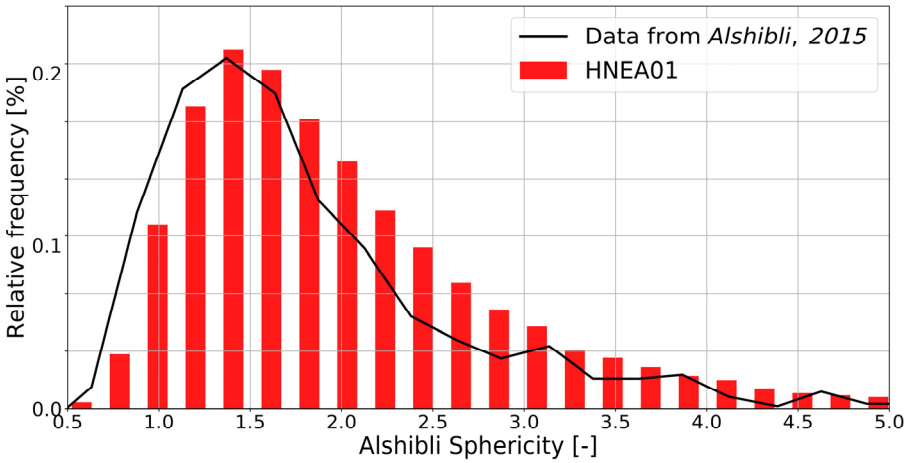

Figure 8: Comparison between the histograms of the Alshibli sphericity (see Table 1) of Hostun sand measured in this work with the data presented in (Alshibli, 2015).

The larger spectrum of shapes contained in the Hostun specimen is also visible in Figure 9, where the Zingg diagram (Zingg, 1935) is used to represent a bivariate distribution of *flatness* and *elongation indexes*. The Hostun specimen data strides three flatness Blott & Pye classes, whereas Caicos is contained in just two classes.

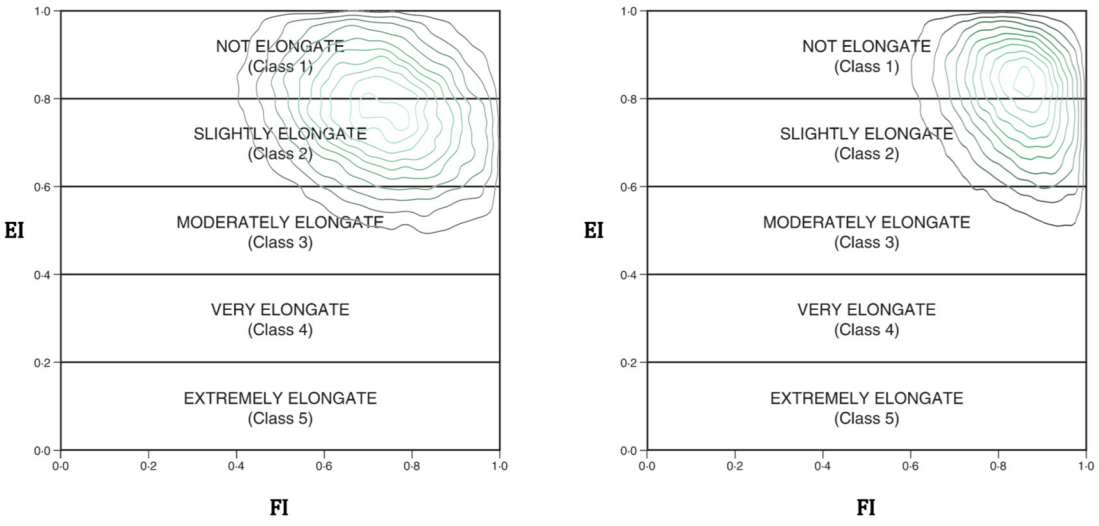

(a) (b)

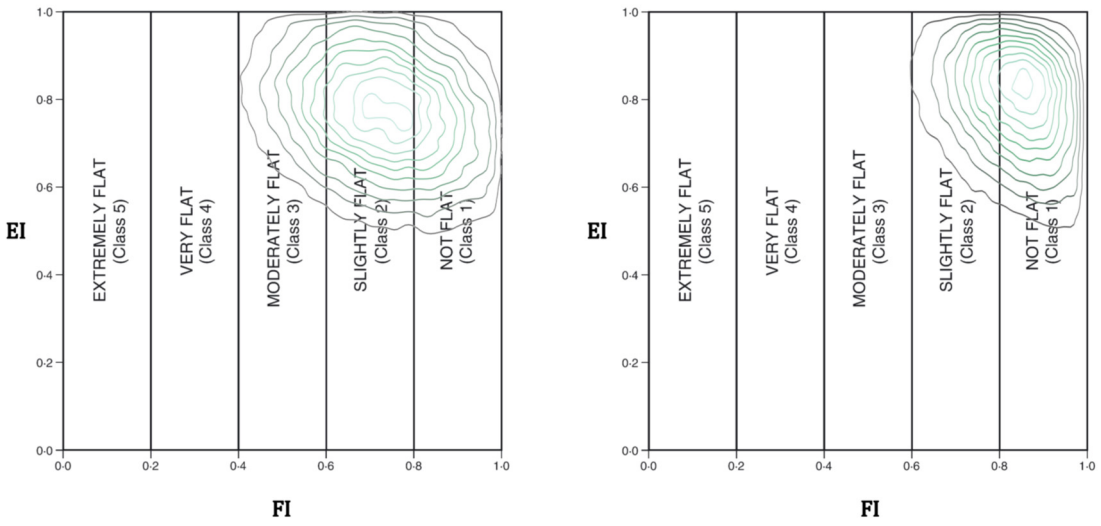

(c) (d)

357 *Figure 9: Bivariate density plot of Hostun (a-c) and Caicos (b-d) shown on the Zingg form space with*
358 *Blott & Pye (2008) classifications for Elongation (a-b) and Flatness (c-d). Isoline spacing is 10%.*

359 ## 4.3 Shape descriptors: correlations

360 The correlations existing between some shape descriptors can be investigated simply plotting a
361 couple of shape descriptors onto different axis in order to explore their distribution on a scatter
362 plot. Since particle shape should convey geometrical information distinct from grain size, shape
363 descriptors independent of particle volume are desirable. In Figure 10, 2D bivariate frequency
364 distributions showing the mutual relationship between the degree of true sphericity and particle
365 volume are plotted. The width of the sphericity marginal distribution at constant volume reduces
366 as volume increases and the number of particles reduces. The mode, on the other hand, appears
367 rather stable despite a slight negative bias towards lower Ψ with size for the artificial Hostun sand
368 (Figure 10a).

369

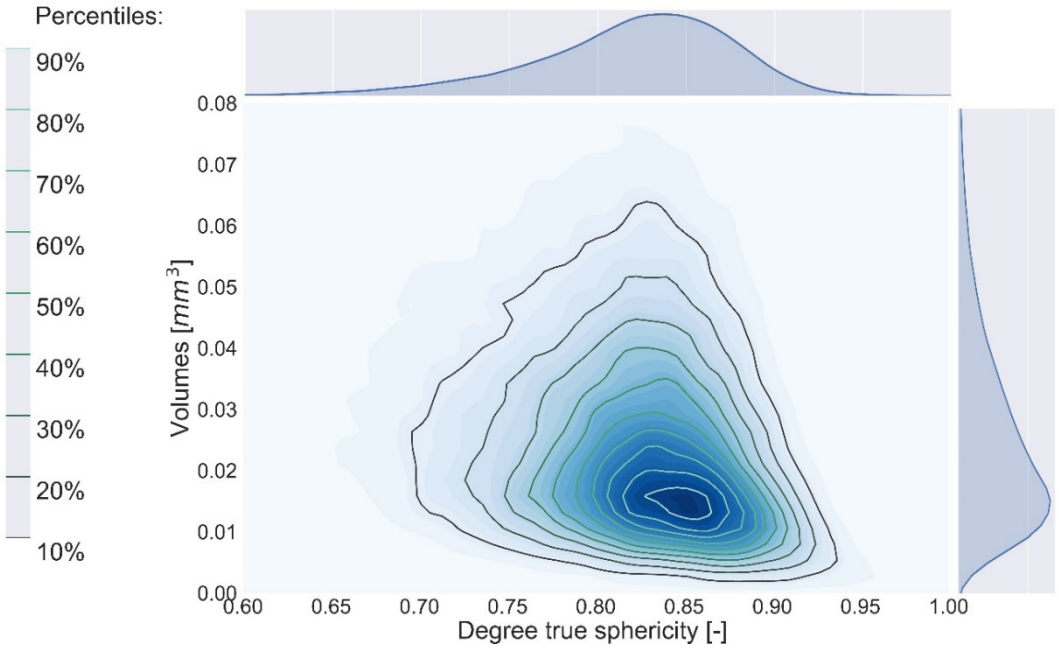

(a)

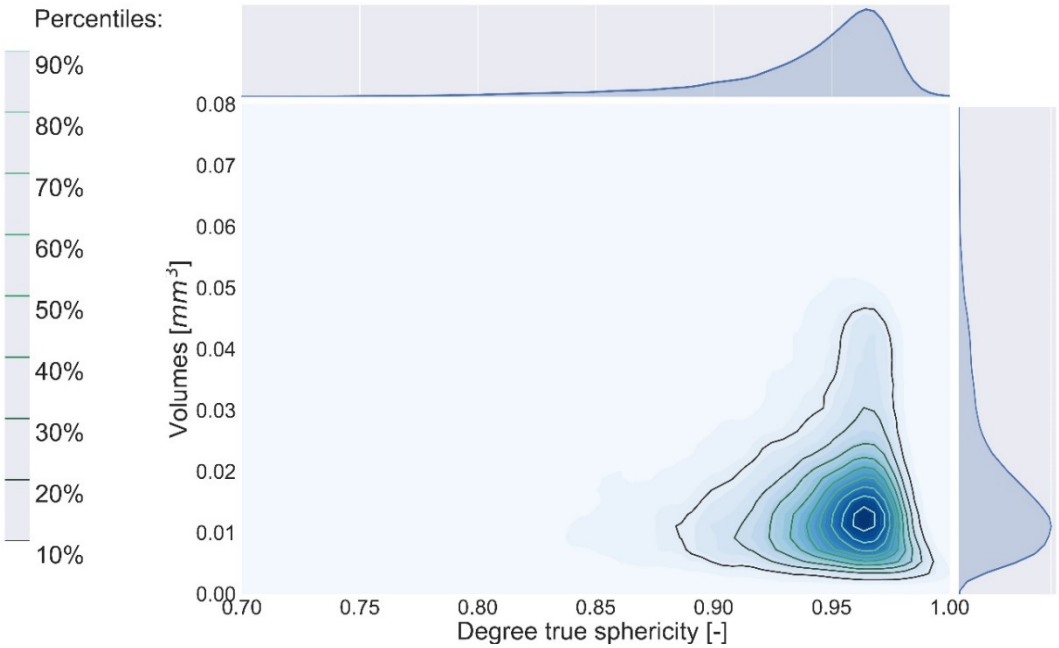

(b)

370 *Figure 10: Relation between true sphericity and particle volume for Hostun sand (a) and Caicos ooids*
371 *(b). Marginal distributions are also shown alongside the axis*

372 Pearson product-momentum correlation coefficients for the shape parameters in specimens
373 HNEA01 and COEA04 are summarized in correlation matrices presented in Table 8 and 9. Ob-
374 serving Table 8 and 9, it appears that the correlation values for the two sands are similar, partic-
375 ularly for the stronger correlations. It is interesting that the *degree of true sphericity* shows a

relatively good correlation with a simple measure like *Operational sphericity*. However, the stronger correlation is with *Convexity*. That strong correlation is indicative of a relatively rotund shape for this sand grains.

On the other hand, Krumbein *intercept sphericity*, Ψ_{int} is not as satisfactory as it is closer to Elongation Index than to either true or operational sphericity. The slight negative correlation between flatness and elongation indexes was already visible in Figure 9. The behaviour of other descriptors is more unexpected: for instance, the sphericity proposed by Alshibli (Ψ_{al}) appears negatively correlated with most other descriptors.

SHAPE DESCRIPTOR	***V***	$\boldsymbol{\Psi}$	***FI***	***EI***	$\boldsymbol{\Psi_{int}}$	$\boldsymbol{\Psi_{op}}$	***Co***	$\boldsymbol{\Psi_{al}}$
Grain volume	1.00	-0.26	0.13	0.09	0.16	0.03	-0.39	-0.20
True Sphericity	-0.26	1.00	0.37	0.26	0.47	0.62	0.84	-0.31
Flatness index	0.13	0.37	1.00	-0.21	0.36	0.34	0.05	-0.80
Elongation index	0.09	0.26	-0.21	1.00	0.83	0.32	0.10	-0.17
Intercept sphericity	0.16	0.47	0.36	0.83	1.00	0.51	0.12	-0.62
Operational sphericity	0.03	0.62	0.34	0.32	0.51	1.00	0.43	-0.33
Convexity	-0.39	0.84	0.05	0.10	0.12	0.43	1.00	0.11
Alshibli Sphericity	-0.20	-0.31	-0.80	-0.17	-0.62	-0.33	0.11	1.00

Table 8: Correlation matrix of the shape parameters for Hostun sand (48.612 grains).

SHAPE DESCRIPTOR	V	Ψ	*FI*	*EI*	Ψ_{int}	Ψ_{op}	*Co*	Ψ_{al}
Grain volume	1.00	-0.07	0.08	0.07	0.10	0.13	-0.28	-0.11
True Sphericity	-0.07	1.00	0.30	0.46	0.59	0.70	0.86	-0.32
Flatness index	0.08	0.30	1.00	-0.22	0.17	0.25	0.15	-0.69
Elongation index	0.07	0.46	-0.22	1.00	0.92	0.56	0.18	-0.37
Intercept sphericity	0.10	0.59	0.17	0.92	1.00	0.67	0.24	-0.65
Operational sphericity	0.13	0.70	0.25	0.56	0.67	1.00	0.48	-0.39
Convexity	-0.28	0.86	0.15	0.18	0.24	0.48	1.00	0.04
Alshibli Sphericity	-0.11	-0.32	-0.69	-0.37	-0.65	-0.39	0.04	1.00

Table 9: Correlation matrix of the shape parameters for Caicos sand (65.056 grains).

4.4 Relation between 2D and 3D shape descriptors

Table 10 and Table 11 show the correlation matrices of true sphericity (3D) and the 2D sphericity proxies listed in Table 3 as measured, respectively, on the *randomly* and *non-randomly* chosen particle projections. Data for Caicos and Hostun is merged in this analysis.

SHAPE DESCRIPTOR	**Ψ**	S_A	S_D	S_C	S_P	S_{KS}
True Sphericity 3D	1.00	0.58	0.61	0.66	0.55	0.49
Area sphericity 2D	0.58	1.00	0.99	0.95	0.72	0.81
Diameter sphericity 2D	0.61	0.99	1.00	0.93	0.65	0.80
Circle ratio sphericity 2D	0.66	0.95	0.93	1.00	0.71	0.77
Perimeter sphericity 2D	0.55	0.72	0.65	0.71	1.00	0.34
KS sphericity 2D	0.49	0.81	0.80	0.77	0.34	1.00

391 *Table 10: Correlation matrix between 3D and 2D sphericity parameters (obtained from randomly ori-*
392 *ented projections). Merged data for Hostun and Caicos, 2000 grains for each one.*

SHAPE DESCRIPTOR	**Ψ**	S_A	S_D	S_C	S_P	S_{KS}
True Sphericity 3D	1.00	0.70	0.69	0.72	0.83	0.36
Area sphericity 2D	0.70	1.00	1.00	0.96	0.80	0.81
Diameter sphericity 2D	0.69	1.00	1.00	0.96	0.80	0.81
Circle ratio sphericity 2D	0.72	0.96	0.96	1.00	0.82	0.79
Perimeter sphericity 2D	0.83	0.80	0.80	0.82	1.00	0.45
KS sphericity 2D	0.36	0.81	0.81	0.79	0.45	1.00

393 *Table 11: Correlation matrix showing 3D and 2D sphericity parameters (obtained from projections ori-*
394 *ented along the minor principal axis). Merged data for Hostun and Caicos, 2000 grains for each one.*

It is noteworthy, but not surprising – given its close relation to elongation – that the Krumbein-Sloss sphericity 2D proxy offers the poorest correlation with the 3D true sphericity measure. The correlation strength for all the other 2D proxies increases significantly when the 2D measurements are taken on oriented (i.e. maximum area) projections. In particular, *perimeter sphericity* (S_P) is the 2D descriptor that appears best correlated with true sphericity (Pearson correlation coefficient equal to 0.83). This perhaps reflects the fact that the definition of *perimeter sphericity* (Table 3) is equivalent to that of true sphericity for the 2D case. For practical purposes, a linear regression line can be drawn (Figure 11) through the data to link the 3D true sphericity with the 2D perimeter sphericity resulting in the expression

$$\psi = 1.075(S_P) - 0.067 \quad (1)$$

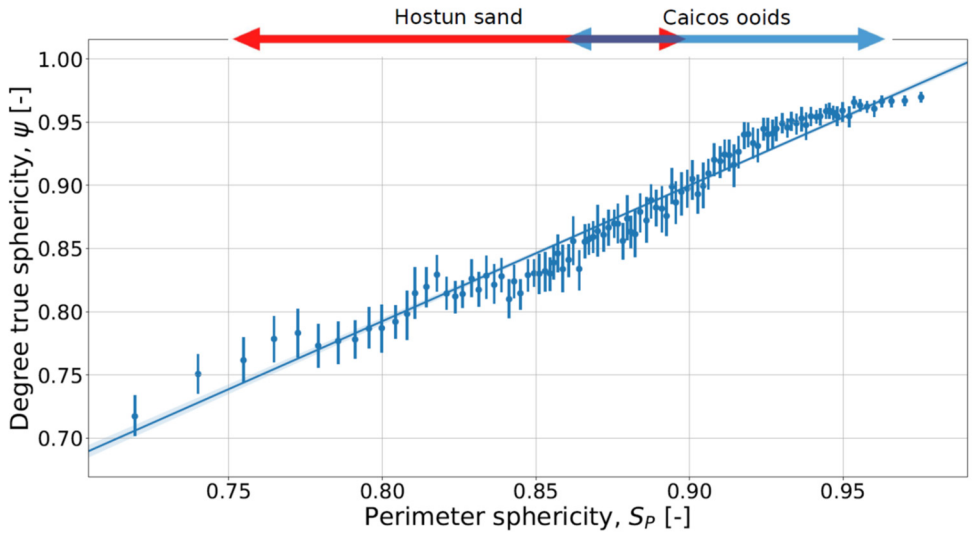

Figure 11: Linear regression line between true sphericity (3D) and perimeter sphericity (2D). The arrows show the ranges (5% and 95% percentiles) of the two sands.

4.5 Statistical convergence

The sand specimens studied in this work contain many thousands grains each. Shape was measured in all of them. This exhaustive procedure was necessary for other studies – not reported here – but will not have been so if the goal was simply shape characterization. Figure 12 shows the deviation from the whole specimen value of the three first statistical moments (i.e. *mean*, *standard deviation* and *skew*) of the true sphericity distribution computed in random example samples of varying size.

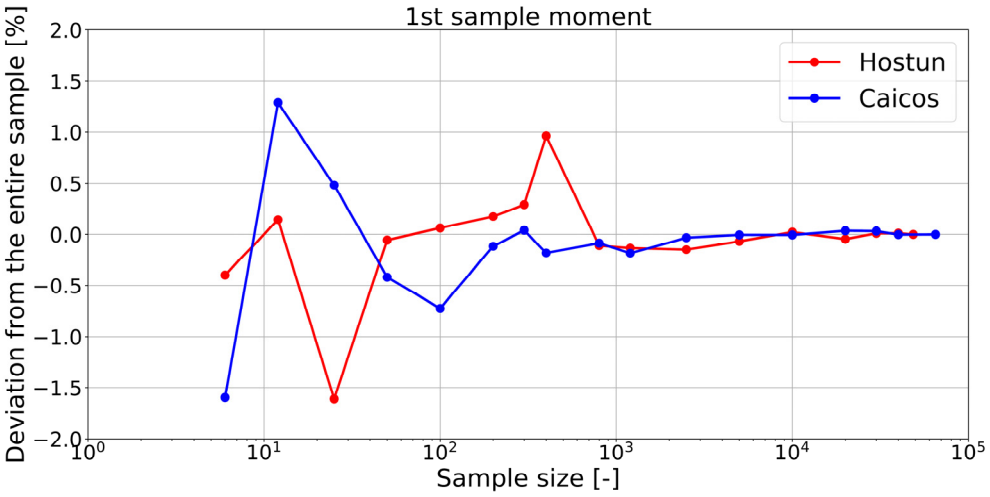

(a)

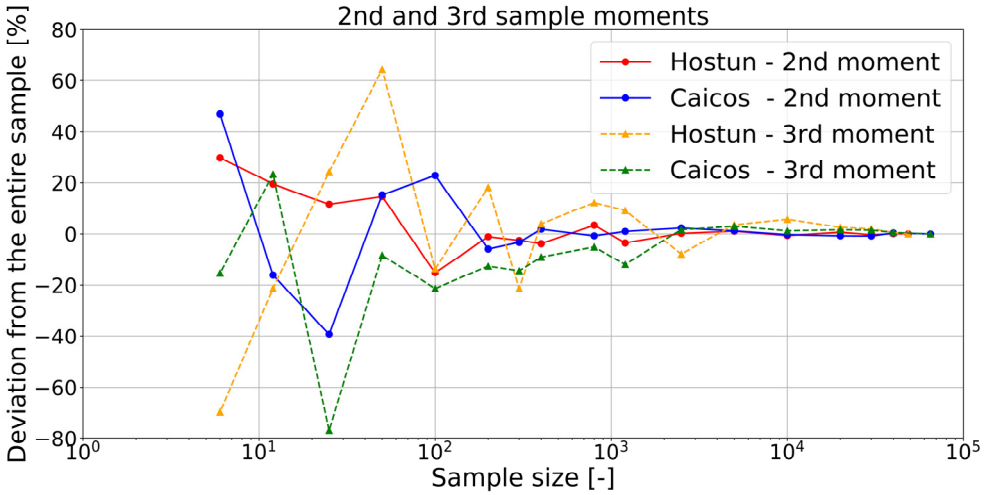

(b)

Figure 12: Evolution of the first and second sample moments with sample size

As expected, it is evident that the error decreases with sample size, and it suggests that sample sizes of at least 1000 particles should be employed to capture shape variability in sands. This number, although far smaller than that used in this study is still one order of magnitude higher of that reported in most 3D studies of sand shape to date.

4.6 Sphericity evolution during triaxial shearing

The sand specimens analysed here were then tested in triaxial compression under a cell confinement of 100 kPa (Andò, 2013). The stress level applied in these tests is well below that required for breakage and indeed no breakage was visible in tomography. Using a reduced subset of grains (2000) a check was made on the evolution of shape parameters during the triaxial test. The summary statistics for some parameters at the final state are reported in Table 12. The averages and standard deviations remain practically unchanged when compared with the initial values (Table 5), particularly for the harder Hostun sand. Minor changes are noted in skew, a statistic that is highly sensitive to changes at the extremes of the distribution. A tiny decrease in particle size is detected in Caicos. These very small changes are consistent with previous work (e.g. Altuhafi and Coop 2011) where insignificant shape change was noted for tests below the onset of particle breakage.

Name	**Mean**	**St. Dev.**	**Skew**	**CV**
	Hostun	*Hostun*	*Hostun*	*Hostun*
	Caicos	*Caicos*	*Caicos*	*Caicos*
Volume (mm^3)	0.028	0.017	1.61	0.62
	0.023	0.014	2.75	0.63
True Sphericity	0.82	0.06	-0.75	0.07
	0.95	0.04	-2.14	0.05
Flatness index	0.73	0.13	-0.17	0.18
	0.84	0.09	-0.74	0.11
Elongation index	0.76	0.12	-0.24	0.16
	0.80	0.11	-0.80	0.14
Intercept sphericity	0.74	0.08	-0.20	0.11
	0.81	0.08	-0.80	0.10

Operational Sphericity	0.58	0.07	-0.15	0.11
	0.72	0.08	-0.62	0.11
Convexity	0.77	0.08	-1.14	0.11
	0.93	0.05	-2.97	0.05
Alshibli Sphericity	1.96	0.91	2.04	0.47
	0.86	0.15	-0.16	0.21

Table 12: Statistics of the 3D shape descriptors for the two sands at the critical state on 2000 grains

5 Conclusion

Measuring how different a sand grain is from a sphere is interesting for a variety of purposes. The sphericity measure proposed by Wadell (1932), true sphericity, was obtained for all grains in two different sand specimens, totalling more than 100 thousand measurements. Together, the values acquired cover the most likely range of this parameter in non-microporous soils. Within the size range explored, true sphericity is independent of particle size. True sphericity appears to be well correlated with 3D convexity and, more usefully, with a 2D measure, perimeter sphericity. This last correlation is sensitive to the particle orientation when the 2D image is acquired, being much stronger when maximum particle projection is used than when random orientation is employed. The traditional Krumbein-Sloss measure of sphericity is poorly correlated with true sphericity.

Acknowledgments. The work here described has been supported by the Spanish Ministry of Economy through grants BIA2014-59467-R and BIA2017-84752-R. The authors are grateful to Prof. Cino Viggiani for his encouragement.

6 References

Alshibli, K.A., Druckrey, A.M., Al-Raoush, R.I., Weiskittel, T., Lavrik, N. V, 2015. Quantifying Morphology of Sands Using 3D Imaging. J. Mater. Civ. Eng. 27. https://doi.org/10.1061/(ASCE)MT.1943-5533.0001246

Altuhafi, F., O'Sullivan, C., Cavarretta, I., 2012. Analysis of an image-based method to quantify the size and shape of sand particles. J. Geotech. Geoenvironmental Eng. 139, 1290–1307. https://doi.org/10.1061/(ASCE)GT.1943-5606.0000855.

Altuhafi, F.N., Coop, M.R., 2011. Changes to particle characteristics associated with the compression of sands. Géotechnique 61, 459–471. https://doi.org/10.1680/geot.9.P.114

Andò, E., 2013. Experimental investigation of microstructural changes in deforming granular media using x-ray tomography. Mechanics. Université de Grenoble.

Andò, E., Hall, S.A., Viggiani, G., Desrues, J., Bésuelle, P., 2012. Grain-scale experimental investigation of localised deformation in sand: A discrete particle tracking approach. Acta Geotech. 7, 1–13. https://doi.org/10.1007/s11440-011-0151-6

Barber, C.B., Dobkin, D.P., 1996. The Quickhull Algorithm for Convex Hulls. ACM Trans. Math. Softw. 22, 469–483.

Barret, P.J., 1980. The shape of rock particle, a critical review. Sedimentology 27, 291–303. https://doi.org/10.1111/j.1365-3091.1980.tb01179.x

Bernard, L., Fave, S., Noirfalise, E., Saragaglia, A., 2011. Visilog 7 Reference Guide, Manual. ed. Noesis S.A., Espace technologique, Route de l'orme, Batiment Mercury 2, 91190 Saint Aubin, France: Noesis S.A.

Blott, S.J., Pye, K., 2008. Particle shape: A review and new methods of characterization and classification. Sedimentology 55, 31–63. https://doi.org/10.1111/j.1365-3091.2007.00892.x

Bowman, E.T., Soga, K., Drummond, W., 2001. Particle shape characterisation using Fourier descriptor analysis. Géotechnique 51, 545–554. https://doi.org/10.1680/geot.51.6.545.40465

Calvetti, F., Prisco, C., Nova, R., 2004. Experimental and Numerical Analysis of Soil – Pipe Interaction. J. Geotech. Geoenvironmental Eng. 130, 1292–1299. https://doi.org/10.1061/(ASCE)1090-0241(2004)130

Cavarretta, I., 2009. The influence of particle characteristics on the behaviour of coarse grained soils. Imperial College London. https://doi.org/10.1680/geot.2010.60.6.413

Chang, C.S., Deng, Y., Meidani, M., 2018. A multi-variable equation for relationship between limiting void ratios of uniform sands and morphological characteristics of their particles. Eng. Geol. 237, 21–31. https://doi.org/10.1016/j.enggeo.2018.02.003

Cho, A.G., Dodds, J., Santamarina, J.C., 2006a. Particle Shape Effects on Packing Density , Stiffness and Strength – Natural and Crushed Sands- Document Summary Number of Words : 4 , 266 Number of Tables : 2 Number of Figures : 11. J. Geotech. Geoenvironmental Eng. 132, 591–602. https://doi.org/10.1061/(ASCE)1090-0241(2006)132:5(591)

Cho, A.G., Dodds, J., Santamarina, J.C., 2006b. Particle Shape Effects on Packing Density , Stiffness and Strength – Natural and Crushed Sands. J. Geotech. Geoenvironmental Eng. 132, 591–602. https://doi.org/10.1061/(ASCE)1090-0241(2006)132:5(591)

Desrues, J., Chambon, R., Mokni, M., Mazerolle, F., 1996. Void ratio evolution inside shear bands in triaxial sand specimens studied by computed tomography. Géotechnique 46, 529–546. https://doi.org/10.1680/geot.1996.46.3.529

Fonseca, J., O'Sullivan, C., Coop, M.R., Lee, P.D., 2012. Non-invasive characterization of particle morphology of natural sands. Soils Found. 52, 712–722. https://doi.org/10.1016/j.sandf.2012.07.011

Hayakawa, Y., Oguchi, T., 2005. Evaluation of gravel sphericity and roundness based on surface-area measurement with a laser scanner. Comput. Geosci. 31, 735–741. https://doi.org/10.1016/j.cageo.2005.01.004

Holubec, I., D'Appolonia, E., 1973. Effect of Particle Shape on the Engineering Properties of

Granular Soils, in: Evaluation of Relative Density and Its Role in Geotechnical Projects Involving Cohesionless Soils. ASTM International, pp. 304–318. https://doi.org/10.1520/STP37879S
Iyer, N., Jayanti, S., Lou, K., Kalyanaraman, Y., Ramani, K., 2005. Three-dimensional shape searching: state-of-the-art review and future trends. Comput. Des. 37, 509–530. https://doi.org/10.1016/j.cad.2004.07.002
Jones, E., Oliphant, T., Peterson, P., 2001. SciPy: Open source scientific tools for Python.
Komba, J.J., Anochie-Boateng, J.K., van der Merwe Steyn, W., 2013. Analytical and Laser Scanning Techniques to Determine Shape Properties of Aggregates. Transp. Res. Rec. J. Transp. Res. Board 2335, 60–71. https://doi.org/10.3141/2335-07
Krumbein, W.C., 1941. Measurement and Geological Significance of Shape and Roundness of Sedimentary Particles. J. Sediment. Res. 11, 64–72.
Krumbein, W.C., Sloss, L.L., 1963. Stratigraphy and Sedimentation, Second Edition. San Francisco.
Lin, C.L., Miller, J.D., 2005. 3D characterization and analysis of particle shape using X-ray microtomography (XMT). Powder Technol. 154, 61–69. https://doi.org/10.1016/j.powtec.2005.04.031
Lin, H., Zheng, S., Lourenço, S.D.N., Jaquin, P., 2017. Characterization of coarse soils derived from igneous rocks for rammed earth. Eng. Geol. 228, 137–145. https://doi.org/10.1016/j.enggeo.2017.08.003
Liu, Q.B., Lehane, B.M., 2013. The influence of particle shape on the (centrifuge) cone penetration test (CPT) end resistance in uniformly graded granular soils. Géotechnique 60, 111–121. https://doi.org/10.1139/t06-037
Lorensen, W.E., Cline, H.E., 1987. Marching cubes: A high resolution 3D surface construction algorithm. ACM siggraph Comput. Graph. 21, 163–169. https://doi.org/10.1145/37402.37422
Mollon, G., Zhao, J., 2013. Generating realistic 3D sand particles using Fourier descriptors. Granul. Matter 15, 95–108. https://doi.org/10.1007/s10035-012-0380-x
Nadimi, S., Fonseca, J., 2017. Single-Grain Virtualization for Contact Behavior Analysis on Sand. J. Geotech. Geoenvironmental Eng. 143, 06017010. https://doi.org/10.1061/(ASCE)GT.1943-5606.0001740
Oliphant, T.E., 2006. Guide to NumPy.
Ouhbi, N., Voivret, C., Perrin, G., Roux, J.-N., 2016. Railway Ballast: Grain Shape Characterization to Study its Influence on the Mechanical Behaviour. Procedia Eng. 143, 1120–1127. https://doi.org/10.1016/J.PROENG.2016.06.150
Ritter, J., 1990. An efficient bounding sphere, Graphics Gems. Academic Press Professional, Inc., San Diego (California).
Rodriguez, J.M., 2012. Particle Shape Quantities and Measurement Techniques – A Review. Luleå Univ. Technol. 57. https://doi.org/https://pure.ltu.se/portal/files/41279547/shape_report_november_2012_A4.pdf
Rorato, R., Arroyo, M., Gens, A., Andò, E., Viggiani, G., 2018. Particle shape distribution effects on the triaxial response of sands : a DEM study, in: Micro to MACRO Mathematical Modelling in Soil Mechanics.
Santamarina, J., Cho, G., 2004. Soil behaviour: The role of particle shape, in: Advances in Geotechnical Engineering. Proceedings of the Skempton Conference. London, pp. 1–14. https://doi.org/http://pmrl.ce.gatech.edu/tools/santamarina_cho_2004.pdf
Schanz, T., Vermeer, P.A., 1996. Angles of friction and dilatancy of sand. Géotechnique 46, 145–151. https://doi.org/10.1680/geot.1996.46.1.145
Suh, H.S., Kim, K.Y., Lee, J., Yun, T.S., 2017. Quantification of bulk form and angularity of particle with correlation of shear strength and packing density in sands. Eng. Geol. 220, 256–265. https://doi.org/10.1016/j.enggeo.2017.02.015
Sun, Y., Indraratna, B., Nimbalkar, S., 2014. Three-dimensional characterisation of particle size and shape for ballast. Geotech. Lett. 4, 197–202. https://doi.org/10.1680/geolett.14.00036
Uday, K. V., Padmakumar, G.P., Singh, D.N., 2013. Some studies on morphology of the coarse-

grained soils. Eng. Geol. 152, 48–55. https://doi.org/10.1016/j.enggeo.2012.10.001
Vaid, Y., Chern, J., Tumi, H., 1985. Confining pressure, Grain angularity and Liquefaction. J. Geotech. Eng. 111, 1229–1235.
Wadell, H., 1935. Volume, Shape, and Roundness of Quartz Particles. J. Geol. 43, 250–280. https://doi.org/10.1086/624298
Wadell, H., 1933. Sphericity and Roundness of Rock Particles. J. Geol. 41, 310–331. https://doi.org/10.1086/624040
Wadell, H., 1932. Volume, Shape, and Roundness of Rock Particles. J. Geol. 40, 443–451.
Yang, J., Luo, X.D., 2015. Exploring the relationship between critical state and particle shape for granular materials. J. Mech. Phys. Solids 84, 196–213. https://doi.org/10.1016/j.jmps.2015.08.001
Zhao, B., Wang, J., 2016. 3D quantitative shape analysis on form, roundness, and compactness with micro-CT. Powder Technol. 291, 262–275. https://doi.org/10.1016/j.powtec.2015.12.029
Zheng, J., Hryciw, R.D., 2015. Traditional soil particle sphericity, roundness and surface roughness by computational geometry. Géotechnique 65, 494–506. https://doi.org/10.1680/geot.14.P.192
Zhou, B., Wang, J., Zhao, B., 2015. Micromorphology characterization and reconstruction of sand particles using micro X-ray tomography and spherical harmonics. Eng. Geol. 184, 126–137. https://doi.org/10.1016/j.enggeo.2014.11.009
Zingg, T., 1935. Beitrag zur Schotteranalyse. Schweizerische Mineral. Petrogr. Mitteilungen. https://doi.org/10.3929/ethz-a-000103455